

Estimation of Gas Condensate Relative Permeability using a Lattice Boltzmann Modelling approach

Josephina Schembre-McCabe^{1,*}, Jairam Kamath¹, Andrew Fager² and Bernd Crouse²

¹Chevron Energy Technology Company, Reservoir and Production Engineering, USA

²Dassault Systèmes, USA

Abstract. Predicting well deliverability loss due to condensate banking requires imbibition gas/oil relative permeability as a function of capillary number. These measurements can be difficult to conduct and are often unavailable. It would be of benefit if reasonable estimates of the imbibition relative permeability can be obtained from commonly available drainage data. We use a multiphase Lattice Boltzmann method to compute drainage and imbibition gas/oil relative permeability for a Berea sandstone core. The computations are done on a 3D digital pore space of the core constructed for micro-CT-scan images. The imbibition calculations are for both displacement and dropout processes, and for a range of capillary numbers. These results are then compared to experimental measurements reported in literature as a function of k_{rg}/k_{ro} and capillary number N_c , and they showed agreement with experimental results for different sandstones.

1 Introduction

A gas condensate system is typically single-phase gas at time of discovery. As the gas/condensate system pressure decreases below the dew point in the near-wellbore region, condensate saturation increases leading to “condensate banking.” The effective gas permeability decreases in the near well region, and this often leads to a large reduction of well productivity [1,2]. The ratio of forces expressed as capillary number (Eq. 1) plays a key role in the degree of impairment [3,4,5].

$$N_c = \frac{U\mu}{\sigma} \quad (\text{Eq. 1})$$

The imbibition relative permeability data needed to model condensate banking phenomena are difficult to measure. They are often obtained by performing steady-state or “pseudo-steady-state” experiments. Reservoir condition steady-state relative permeability tests that capture the effect of rock type, flow velocities and near-well bore conditions are especially complex and time consuming. “Pseudo-steady state” relative permeability experiments with reservoir and synthetic fluids that match liquid concentration, viscosity ratio and interfacial tension of the condensate [6,7] are often used. These experiments require fitting to a relative permeability model to obtain curves as function of saturation. In general, imbibition data to model condensate banking are often unavailable. It would be of benefit if reasonable estimates of the imbibition relative permeability can be obtained from commonly available drainage data.

The objective of this work is to test the capabilities of Lattice Boltzmann based multi-phase fluid flow simulation to model drainage and imbibition gas/oil relative permeability, to investigate the effects of different methods of establishing condensate saturation at the pore scale (displacement, dropout), and the effects of capillary

number. A high-resolution 3D image of a Berea sandstone is used to test the simulation method, and the results are compared with data obtained from literature.

2 Methodology

2.1 Sample Imaging

We use a micro-CT device to create a 3D image of a Berea Sandstone sample. Figure 1-left shows one 2D slice perpendicular to flow (1024x1024 pixels) in original grey scale. The slice represents a 5mm diameter plug and has a resolution of 2.6 $\mu\text{m}/\text{voxel}$. Figure 1-right shows the same slice in binary scale after segmentation. The segmentation of the image was performed using an in-house enhanced histogram thresholding method [8].

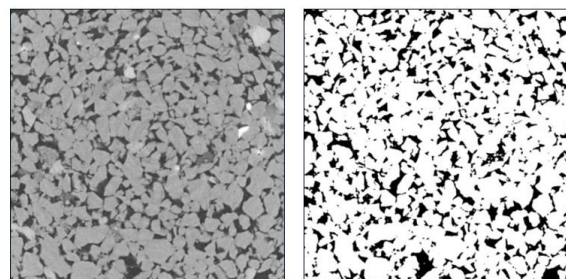


Fig. 1. Two-dimensional section of scans for the Berea Sandstone used in this work: original grey scale (left) and segmented image (right)

The simulations described in the next section were performed for a sub-volume (600x600x600) whose grain- and pore- space visualizations are shown in Figure 2.a (grain space) and 2.b (pore space). The sub-volume had a connected porosity of 17.8% with a critical pore throat radius of 8.3 μm (3.2 voxels). The critical pore throat radius is a measure of pore size. It is defined as the radius of the largest sphere that can start from a face of the rock and find its way within the pore space to the other,

* Corresponding author: jschembremccabe@chevron.com

opposing face. Any sphere with a radius larger than the critical throat radius will become stuck within the pore space. For a cubic 3D geometry, it is measured in all 3 directions. Here the critical throat radius is only reported for the flow direction. The simulated permeability and total porosity was 670 mD and 22 %.

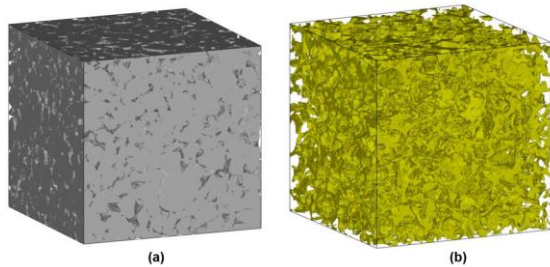


Fig. 2: Visualization of (a) grain and (b) pore space of the 3D model used for all simulation.

2.2 Numerical Modelling Approach

The numerical modelling approach used in this study consists of a multiphase Lattice Boltzmann method (LBM) where condensate dropout and its effects on two-phase flow are investigated and compared to a traditional displacement-based method. LBM has been recently used for directly solving flow scenarios at pore-scale within porous media, particularly for petroleum reservoir rock systems [9,10].

LBM is based on kinetic theory and solves a discrete form of the Boltzmann transport equation. The explicit method often operates on a cubic lattice. This allows for local compute operations with good parallel efficiency. LBM based fluid solvers are considered competitive alternatives to traditional Navier-Stokes PDE-based numerical methods [11-16].

The solver used for this work is based on an extension of the multiphase Shan-Chen model (SC-LBM) [17]. The model used here was recently extended to improve numerical stability and accuracy under the operating conditions required for digital rock workflows, low resolution and low numerical viscosity [18,19]. In the model fluid phase separation is the result of interaction forces between fluid components while wettability is determined by interaction forces between fluid and pore walls.

The pore-solid interface is defined by triangular surface elements, or surfels, which allows for high fidelity representation of the surface. The usage of surfels increases accuracy of near-wall fluxes and is a unique feature of the model used in this work [20,21]. This allows for a relatively coarse number of grid cells to be used for resolving the critical throats of a rock volume, making computational cost of practical rock volumes manageable.

2.3 Numerical Modelling Setup

Two multi-phase flow modelling setups were used to generate gas/condensate relative permeability curves.

The first corresponds to steady-state relative permeability displacement. In the second setup, the drop-out of condensate is modelled, and the effective permeability of both gas and condensate is calculated as a function of saturation and capillary number.

2.3.1. Relative Permeability -- Displacement

A steady-state relative permeability displacement method is used here to simulate both drainage and imbibition displacements. Gas displaces condensate in drainage, while condensate displaces gas in imbibition. Periodic boundary conditions and a driving force are applied in the flow direction, while no-flow boundary conditions are used in the direction transverse to flow. Additional details for this method can be found in [9].

2.3.2 Relative Permeability -- Dropout

In a physical gas condensate system, the liquid condensate phase develops through the spontaneous condensation or dropout of components initially in gas. The dropout of the liquid condensate phase occurs from a state change (typically a pressure reduction) of the system. To model this mechanism in this simulation methodology, condensate mass is uniformly introduced into the gas filled pore space as a new fluid component using a volumetric exchange process. In each voxel a source term introduces condensate mass while a sink term simultaneously removes an equal amount of gas. This is done with a uniform rate of exchange in all gas phase voxels. Initially, the condensate component remains dissolved as the minor component in the gas phase, but as the described exchange process continues to introduce condensate mass and increase condensate density, the interaction forces between the gas and condensate components naturally lead to the spontaneous formation of a liquid condensate phase. Figure 3 shows a diagram of the condensation model in which condensate is introduced in the gas filled pores.

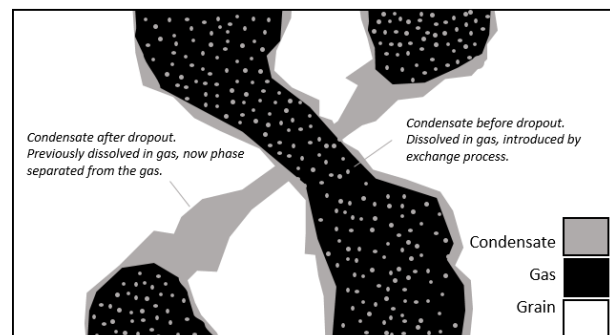


Fig. 3. Diagram of the condensate dropout method

The little condensate points in the gas phase indicate dissolved condensate component in the numerical simulation that have been introduced by the exchange process. After forming a separate phase (i.e. dropping out) the condensate phase is shown to have migrated to and collected along the pore walls. This is representative of condensate being the wetting phase and in agreement with the film-wise process observed in micromodels [22]. Similar to the displacement method a body force is used

to drive flow through the rock over the course of a dropout simulation.

Figure 4 describes the progression of a dropout simulation. The simulation starts at the initial saturation state. The dropout method is initially off. During this step the time behaviour of relevant flow quantities are measured. When these quantities are determined to be converged in time the permeability of all phases, gas and condensate, is measured. Typically, only gas is mobile at the initial saturation state. After measuring permeability, the dropout method is turned on. When the dropout method is on the condensate saturation increases and gas saturation decreases correspondingly. The dropout process continues until a predefined saturation is achieved. When the saturation threshold is achieved the dropout method is turned off and the convergence and permeability measurement step is performed again. The saturation remains constant during this step. Once this step is complete the dropout method is turned on again. The simulation continues to alternate the dropout step and the convergence step until only the condensate phase is mobile and the gas phase is determined to be immobile.

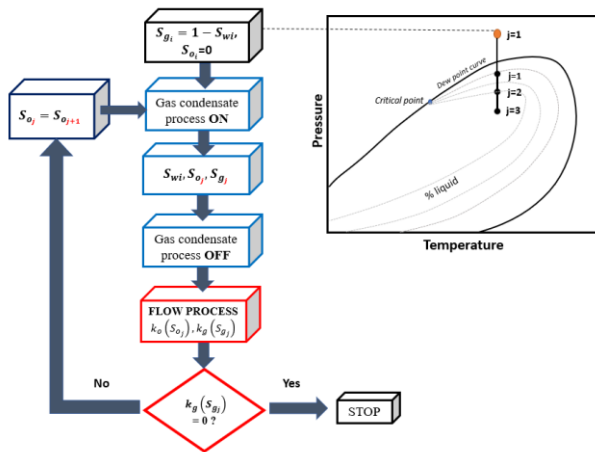


Fig. 4. Diagram showing process for computing Gas/Oil (dropout) relative permeabilities

2.3.3 Modelling Conditions

In this study 5 simulations were performed using the Berea Sandstone 3D model shown in **Figure 2**. **Table 1** provides a list of the simulations performed. In all simulations the liquid condensate is assigned to be the wetting fluid while the gas is assigned as the non-wetting fluid. Pressure, temperature and overall composition will make viscosities different for different fluid systems, in this case the average of the range considered for condensate dynamic viscosity to gas viscosity ratio is 10.

Using the steady-state displacement method both drainage and imbibition condensate/gas simulations are performed. In the drainage simulation gas is the displacing fluid. In the imbibition simulation the liquid condensate is the displacing fluid. Three condensate dropout simulations are also performed. **Table 1** shows the prescribed gas capillary number used for each simulation. The gas capillary number is defined as:

$$N_{c,gas} = \frac{U_t \mu_{gas}}{\sigma} \quad (\text{Eq. 2})$$

Where the total Darcy velocity (U_t) is the sum of the gas and condensate Darcy velocities (Eq. 3). This is held constant throughout a simulation to maintain constant flow rate.

$$U_t = U_g + U_c \quad (\text{Eq. 3})$$

The total Darcy velocity is chosen so that the prescribed gas capillary number is achieved when the condensate phase is immobile and only the gas phase is flowing. For drainage this occurs at the end of the displacement, when all mobile oil has been removed. For both the imbibition displacement and dropout simulations this occurs at the beginning of the simulation when only gas is flowing.

Table 1 : List of Runs performed on Berea 3D Model (**Fig. 2**)

Run	Method	$N_{c,gas}$
1	Steady-State Drainage	1×10^{-5}
2	Steady-State Imbibition	1×10^{-6}
3	Condensate Dropout	1×10^{-6}
4	Condensate Dropout	1×10^{-5}
5	Condensate Dropout	5×10^{-5}

3 Results

3.1 Numerical Simulations on 3D Berea Model

In this section, results from the simulations described above are presented and discussed. **Figure 5** compares the result of a drainage gas/oil relative permeability simulation for a capillary number of 1×10^{-5} with results from literature representing low and high capillary numbers [23,24]. The results from simulation are in the range between these two boundaries.

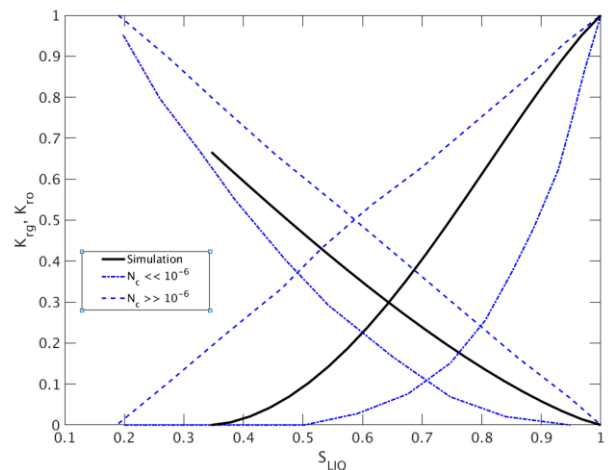


Fig. 5. Comparison of Drainage Oil/Gas relative permeability obtained from run 1 (black) and ranges suggested for sandstones between low capillary number (solid blue line) and high capillary number (dashed blue line).

Figure 6 compares imbibition gas and condensate relative permeabilities obtained from different mechanisms at same capillary number: the dashed line depicts curves where displacement of gas by liquid condensate occurs (run 2); while the solid line shows curves for the case where gas is replaced by liquid condensate using the dropout method (run 3).

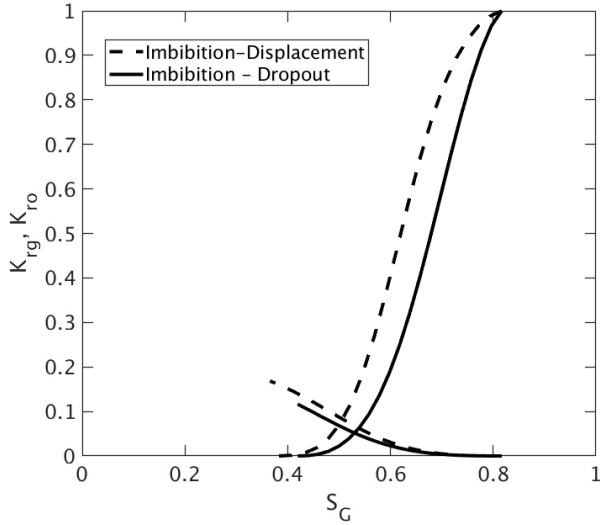


Fig. 6. Comparison of Oil/Gas Relative Permeabilities obtained by Displacement (run 2) and Gas Condensate formation (run 3) at $N_c = 1 \times 10^{-6}$

Condensate relative permeability is lower in the dropout case. This could be due to more regions of disconnected condensate saturation. Dropout gas relative permeability values are also lower. This could be due to the relatively uniform introduction of condensate into both large and small pores by the dropout method. This would cause the gas phase to breakup sooner than in the displacement method where the preference is for condensate to fill small pores first and preserve the connectivity of the gas phase.

Figure 7 compares k_{rg}/k_{ro} data for drainage displacement, imbibition displacement, and imbibition dropout. The drainage displacement values are much higher than the imbibition values, and the differences between the two methods of imbibition are relatively minor. At the end of each simulation shown in figure 6, when the displaced fluid is trapped, the capillary number based on the displacing fluid is the same. For drainage (run 1) this is $N_{c,gas} = 1 \times 10^{-5}$. For both imbibition simulations (run 2 & 3) this is $N_{c,cond} = 1 \times 10^{-5}$.

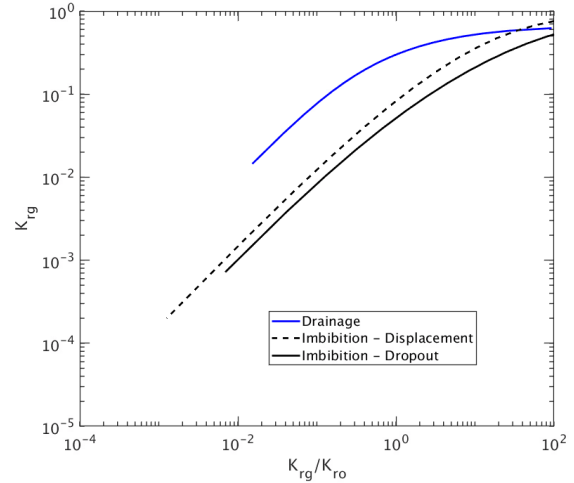


Fig. 7. Gas Relative permeability as a function of k_{rg}/k_{ro} for drainage and imbibition (displacement, dropout)

Our findings of small differences between displacement and dropout imbibition data are consistent with those of Henderson et al. [4].

Figure 8 shows four snapshots of gas and liquid dropout distribution for run 3 at four different saturations steps; liquid dropout appears in different regions of the 3D volume as the simulation progresses towards increased liquid condensate saturations.

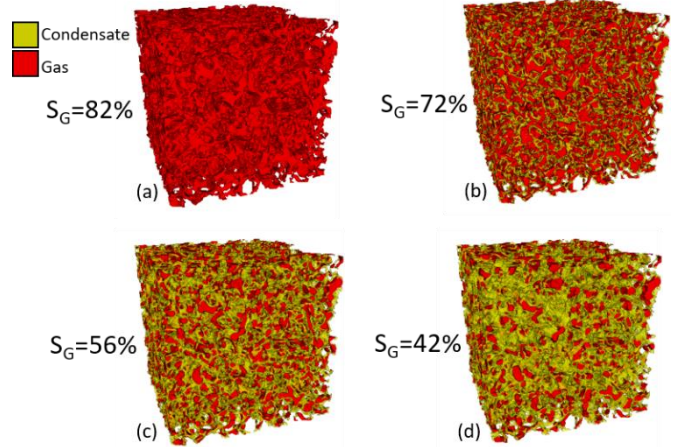


Fig. 8. Snapshot of gas and liquid dropout distribution at different gas saturation stages in run 3 at $N_c = 1 \times 10^{-6}$ (Table 1).

Figure 9 shows gas and condensate relative permeability for different capillary numbers (runs 3, 4 and 5 in Table 1). **Fig. 10** plot same data from Fig. 8 in semilog scale, which shows critical condensate saturation in the range of 20% for the lowest capillary number tested in this study ($N_c = 1 \times 10^{-6}$); because we set a target condensate saturation in this range, the evolution towards lower critical condensate saturations at larger capillary numbers is not resolved; however, the trend of the condensate relative permeability in this plot suggests that critical condensate saturation decreases with increasing capillary number.

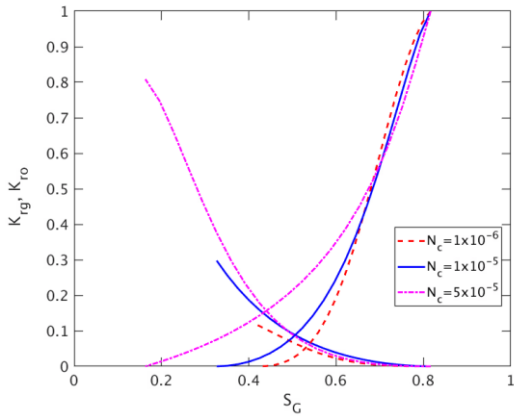


Fig. 9. Gas Condensate Relative Permeability obtained from runs 3, 4 and 5 (Table 1).

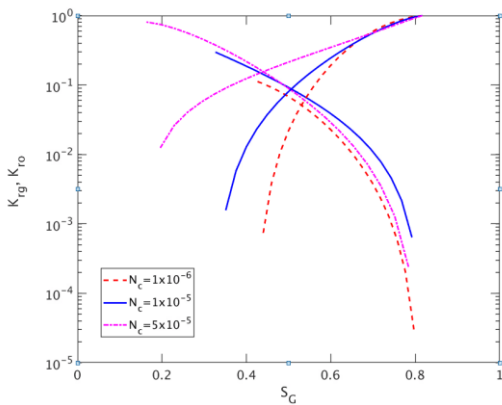


Fig. 10. Gas Condensate Relative Permeability from Fig. 8 (semi log).

Fig. 11 shows data from Fig. 8 in the $k_{rg} = f(k_{rg}/k_{ro})$ which is used to model gas condensate by developing relative permeability at different capillary numbers [1, 5]. It shows that gas mobility increases with increasing capillary number, which is an expected well-known trend [2,5,7]. There is some discrepancy in the high k_{rg}/k_{ro} space and this needs to be further explored.

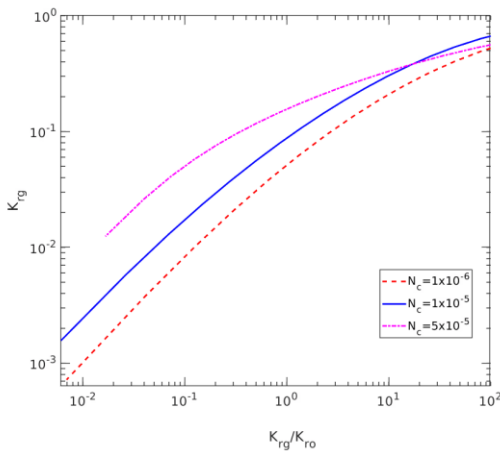


Fig. 11. Gas Relative permeability as a function of Gas/Oil Relative Permeability ratio from relative permeability obtained from runs 3, 4 and 5 (Fig. 4, Table 1).

Figure 12 shows visualizations of the gas phase at the residual gas condition of each capillary number simulated with the dropout method. The visual shows that much of the gas is disconnected and that the amount of gas decreases with increasing capillary number.

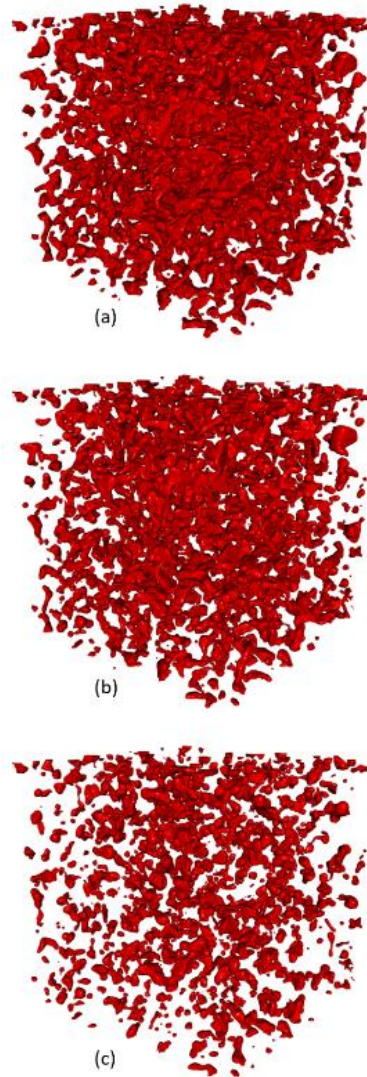


Fig. 12. Visualization showing locations of trapped gas for (a) run #3 at $N_c=1e-6$, (b) run 4 at $N_c=1e-5$, and (c) run 5 at $N_c=5e-5$.

Figure 13 shows the average blob volume measured at the same residual gas conditions. As capillary number increases the size (volume) of gas blobs decreases. The range of values of trapped gas saturations are in line with the 25-45% range reported in the literature [23].

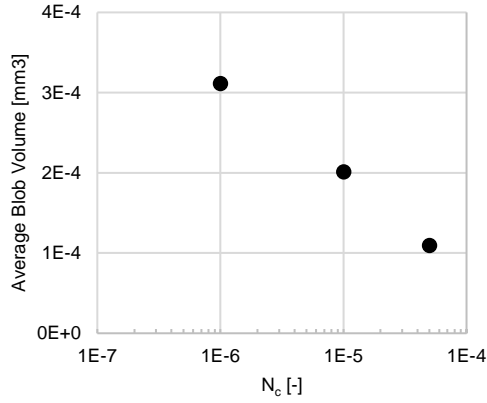


Fig. 13. Average blob volume for each capillary number simulated with the dropout method (run 3 to 5). Blob volume measured at the residual gas condition of each simulation.

Figure 14 shows iso-surface visualizations of the gas blob locations. These are shown for both the displacement and dropout method. A gas saturation of $S_G=48\%$ is shown. These are intermediate saturation states where both gas and condensate are still flowing. The blob color denotes blob volume with the largest gas blobs colored as red and the smallest colored as blue. The deep red colored gas blobs represent the largest gas blobs. These blobs are often fully connected from inlet to outlet and associated with high gas relative permeability. It is observed that the displacement method leads to a gas phase that has a better connectivity than the dropout method. This is consistent with the observation that the gas permeability curve generated by the displacement method is overall higher than that generated by dropout method as shown in **figure 6**.

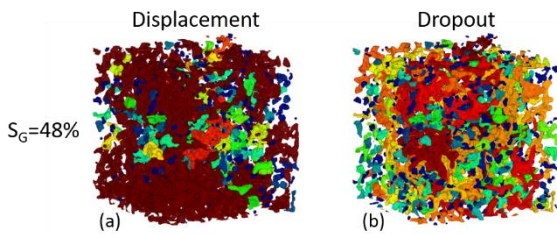


Fig. 14. Visualization showing locations and volume of gas blobs. Color denotes blob volume. Largest gas blobs colored red. Smallest gas blobs colored blue. (a) shows displacement (run #2) while (b) shows dropout (run #3).

3.2 Comparison with published data

In this section, the results presented in the previous section in **Fig. 11** are compared with results reported in literature for sandstone in the form of $k_{rg} = f(k_{rg}/k_{ro})$. The comparison covers the range of capillary numbers [4,26,27,28] that include the capillary number used in this study (**Table 2**). The data compiled was collected in Berea or reservoir sandstone with porosity ranging between 17 and 25%, and permeabilities between 50 and 500 mD. Most of the data were obtained using the Steady State method, generally by fixing target gas condensate ratio (GCR) at each step. Cable et al [25] and Kumar et al [28],

used pseudo-state method to measure relative permeability. Regarding the fluid properties, some of these studies used mixtures match fluids at reservoir conditions and/or reservoir fluids, the oil/gas viscosity ratio ranged between 7 and 40 for the cases we used for comparison.

Figure 15 compares run 3 ($N_c=1 \times 10^{-6}$) with data reported for capillary numbers ranging between 1×10^{-6} and 5×10^{-6} [4,26,27,28,31]. We see good agreement between the data reported for this range and the simulation results.

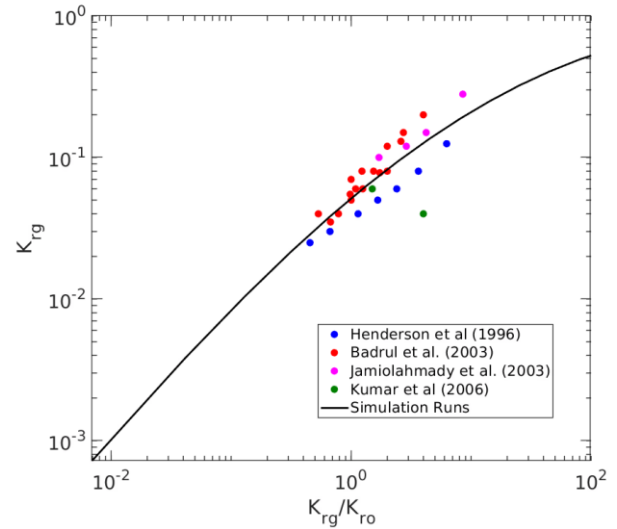


Fig. 15. Gas Relative permeability as a function of k_{rg}/k_{ro} . Comparison of Simulation run # 3 ($N_c = 1 \times 10^{-6}$) with data published in the literature for range covering the capillary number condition ($1 \times 10^{-6} \leq N_c < 5 \times 10^{-6}$)

Figure 16 compares run 4 ($N_c=1 \times 10^{-5}$) with data reported for capillary numbers ranging between 5×10^{-6} and 2×10^{-5} [4,26,28,30,31]. For this range, we observed more variability in the data reported in literature compared to the previous case at lower capillary number. And yet, the simulation results show good agreement with the results reported in literature

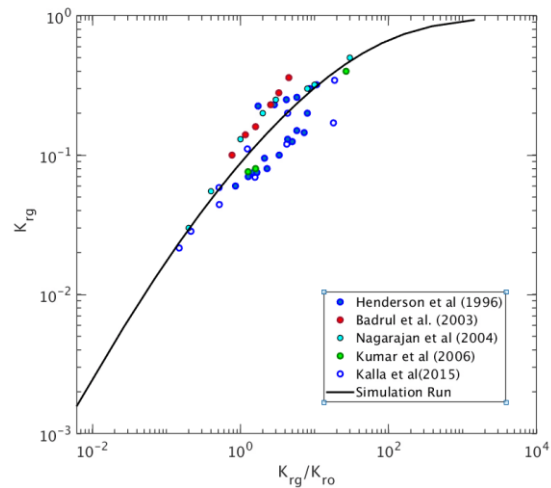


Fig. 16. Gas Relative permeability as a function of k_{rg}/k_{ro} . Comparison of Simulation run 4 ($N_c = 1 \times 10^{-5}$) with data

published in the literature for range covering the capillary number condition ($5 \times 10^{-6} \leq N_c < 2 \times 10^{-5}$).

Figure 17 compares run 5 with data reported for capillary numbers larger than 2×10^{-5} [25,31]. Even though we have less data to compare in this range and experimental data shows uncertainty, we see a good agreement between the simulation results and the range of data reported

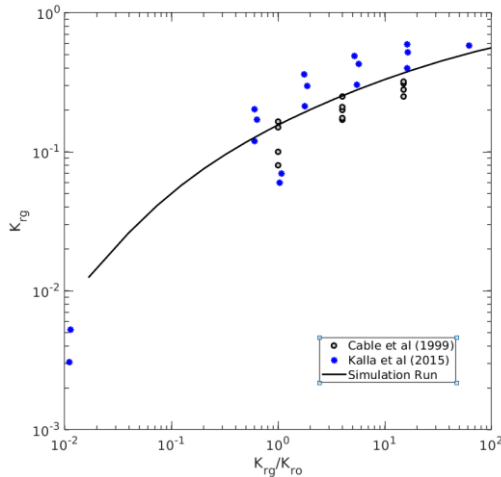


Fig. 17. Gas Relative permeability as a function of k_{rg}/k_{ro} . Comparison of Simulation run 5 ($N_c = 5 \times 10^{-5}$) with data published in the literature for range covering the capillary number condition ($N_c \geq 2 \times 10^{-5}$).

4 Conclusions

Multiphase flow LBM calculations of imbibition gas/oil relative permeability for a Berea sandstone gave promising results -

- The calculated gas relative permeability as a function (k_{rg}/k_{ro} , N_c) was in line with experimental results for different sandstones
- There were minor differences between displacement and dropout methods of establishing a wetting condensate saturation. This is as expected and consistent with the literature.

Future work will need a careful comparison where there is computed and measured drainage and imbibition data on the same sample. If the results are still promising, LBM offers a way to calculate the imbibition gas/oil relative permeability data needed to model effects of condensate banking from commonly available drainage experiments.

5 Nomenclature

k_{rg} = gas relative permeability
 k_{ro} = oil or gas condensate relative permeability
 S_{LIQ} = liquid saturation
 S_g = gas saturation
 S_{gr} = residual gas saturation
 S_{oc} = critical gas condensate saturation
 S_{org} = residual oil (to gas) saturation
 U = velocity

μ = viscosity
 σ = interfacial tension
 N_c = capillary number

Acknowledgments

We would like to acknowledge the support of Chevron Corp and Dassault Systèmes to allow the publication of this work.

References

1. H. L. Chen, S. D. Wilson, and T. G. Monger-McClure, "Determination of Relative Permeability and Recovery for North Sea Gas Condensate Reservoirs," SPE 30769, *SPE Annu. Tech. Conf. and Exhib.*, Dallas, TX, USA, Oct 22-25, 1995.
2. J. Kamath, "Deliverability of Gas-Condensate Reservoir – Field Experiences and Prediction Techniques," *JPT*, pp 94- 99, Apr 2007.
3. W. Boom, K. Wit, A. M. Shulte, S. Oedai, J.P.W. Zeelenberg and J. G. Maas, "Experimental Evidence for Improved Condensate Mobility at Near-wellbore Flow Conditions," SPE 30766, *SPE Annu. Tech. Conf. and Exhib.*, Dallas, TX, USA, Oct 22-25, 1995.
4. G. D. Henderson, A. Danesh, D. H. Tehrani, S. Al-Shaidi, and J. M. Peden, "Measurements and Correlation of Gas Condensate Relative Permeability by the Steady-State Method," *SPE J.*, vol 6, pp 191-201, 1996.
5. G. A. Pope, W. Wu, G. Narajanaswamy, M. Deslhad, M. Sharma, and P. Wang, "Modeling Relative Permeability Effects in Gas Condensate Reservoirs," SPE 49266, *SPE Annu. Tech. Conf. and Exhib.*, New Orleans, LA, Sept 27-30, 1998.
6. C. H. Whitson, Ø. Fevang, and A. Sævareid, "Gas condensate Relative Permeability for Well Calculations," *Transport in Porous Media*, vol. 52, pp 279-311, 2003.
7. V. Kumar, V. Bang, G.A. Pope, M.M. Sharma, P.S. Ayyalasomayajula, and J. Kamath, "Chemical Stimulation of Gas/Condensate Reservoirs," SPE 102669, *SPE Annu. Tech. Conf. and Exhib.*, San Antonio, Texas, USA, Sept 24-27, 2008.
8. J. M. Schembre-McCabe and J. Kamath, "Using Digital Rock Technology to Quality Control and Reduce Uncertainty in Relative Permeability Measurements," *Petrophysics*, vol 59, no. 1. pp 44-53, 2018.
9. G. R. Jerauld, J. Fredrich, N. Lane, Q. Sheng, B. Crouse, D. M. Freed, A. Fager, and R. Xu, "Validation of a Workflow for Digitally Measuring Relative Permeability," SPE 188688, *2017 SPE Abu Dhabi Int. Pet. Exhib. & Conf.*, Abu Dhabi, U.A.E., Nov. 13-16, 2017.
10. H. Andrä, N. Combaret, J. Dvorkin, E. Glatt, J. Han, M. Kabel, Y. Keehm, F. Krzikalla, M. Lee, C. Madonna, M. Marsh, T. Mukerji, E. H. Saenger, R. Sain, N. Saxena, S. Ricker, A. Wiegmann, X. Zhan, "Digital rock physics benchmarks—part II:

- Computing effective properties,” *Comp. Geosci.*, vol. 50, no. 33, pp 33-43, 2013.
11. S. Chen and G. Doolen, “Lattice Boltzmann method for fluid flows,” *Annu. Rev. Fluid Mech.*, vol. 30, no. 1, pp 329-264, 1998.
 12. S. Chen, H. Chen, D. Martinez, and W. Mattheus, “Lattice Boltzmann model for simulation of magnetohydrodynamics,” *Phys. Rev. Lett.*, vol. 67, no. 27, pp. 3776-3779, Dec. 1991.
 13. H. Chen, S. Chen, W. Matthaeus, “Recovery of the Navier - Stokes equations using a lattice-gas Boltzmann method,” *Phys. Rev. A*, vol. 45, no. 8, pp R5339-R5342, Apr. 1992.
 14. Y. Qian, D. d’Humières, P. Lallemand, “Lattice BGK models for Navier-Stokes equation,” *Europhys. Lett.*, vol. 17, no. 6, pp 479-484, Feb. 1992.
 15. H. Chen, C. Teixeira, and K. Molvig, “Digital physics approach to computational fluid dynamics: some basic theoretical features,” *Intl. J. Mod. Phys. C*, vol. 8, no. 4, pp. 675-684, 1998.
 16. H. Chen, “Volumetric formulation of the lattice Boltzmann method for fluid dynamics: Basic concept,” *Phys. Rev. E*, vol. 58, no. 3, pp. 3955-3963, Sep. 1998.
 17. X. Shan and H. Chen, “Lattice Boltzmann model for simulating flows with multiple phases and components,” *Phys Rev E*, vol. 47, no. 3, p. 1815-1819, Mar. 1993.
 18. H. Otomo, H. Fan, R. Hazlett, Y. Li, I. Staroselsky, R. Zhang, R., and H. Chen, H., “Simulation of Residual Oil Displacement In A Sinusoidal Channel With The Lattice Boltzmann Method,” *Comptes Rendus Mécanique*, vol. 343, no. 10, pp. 559–570, 2015.
 19. H. Otomo, H. Fan, Y. Li, M. Dressler, I. Staroselsky, R. Zhang, and H. Chen, “Studies Of Accurate Multi-Component Lattice Boltzmann Models On Benchmark Cases Required For Engineering Applications,” *Jour. Comp. Sci.*, vol 17, pp. 334–339, 2016.
 20. H. Chen, C. Teixeira, and K. Molvig, “Realization of Fluid Boundary Conditions via Discrete Boltzmann Dynamics,” *Intl. J. Mod. Phys. C*, vol. 9, p. 1281, 1998.
 21. B. Crouse, D. M. Freed, N. Koliha, G. Balasubramanian, R. Satti, D. Bale, and S. Zuklic, “A Lattice-Boltzmann Based Method Applied to Digital Rock Characterization of Perforation Tunnel Damage,” SCA 2016-058, *Int. Symp. Soc. Core Analysts*, Snow Mass, CO, USA., Aug. 2016.
 22. A. Danesh, G. D. Henderson, and J. M. Peden, “Experimental Investigation of Retrograde Condensation in Porous Media at Reservoir Conditions,” SPE 18316, *SPE Annu. Tech. Conf. and Exhib.*, Houston, TX, Oct.2-5, 1988.
 23. G. Jerauld, “Prudhoe Bay Gas/Oil Relative Permeability,” *SPE Res. Eng.*, Feb 1, pp. 66-73, 1997.
 24. S. C. M. Krevor, R. Pini, L. Zuo, and S. M. Benson, “Relative Permeability and trapping of CO₂ and water in Sandstone rocks at reservoir conditions,” *Water Resour. Res.*, vol. 48, no. 2, Feb. 2012.
 25. A. Cable, R. Mott, and M. Spearing, “Experimental Techniques for the Measurement of Relative Permeability and In-Situ Saturation in Gas Condensate Near Wellbore and Drainage Studies,” SCA 9928, *Int. Symp. Soc. Core Analysts*, Golden, CO, USA, 1999.
 26. M. J. Badrul, W. S. Ucok, and L. L Robert, “Effect of Permeability Distribution and Interfacial Tension on Gas Condensate Relative Permeability: An Experimental Study,” SPE 80551, *SPE Asia Pacific Oil and Gas Conf. and Exhib.*, Jakarta, Indonesia, Apr. 15-17, 2003.
 27. M. Jamiolahmady, A. Danesh, G. Henderson, and D. Tehrani, D., “Variations of Gas-Condensate Relative Permeability with Production Rate at Near Wellbore Conditions: A General Correlation,” SPE 83960, *SPE Offshore Europe Conf.*, Aberdeen, UK, Sep. 2-5, 2003.
 28. V. Kumar, G. A. Pope, and M. M. Sharma, “Improving the Gas and Condensate Relative Permeability Using Chemical Treatments,” SPE 100529, *SPE Gas Technol. Symp.*, Calgary, Alberta, Canada, May 15-17, 2006.
 29. A. Sævareid, C. H. Whitson, and Ø. Fevang, “An Engineering Approach to Measuring and Modeling Gas Condensate Relative Permeabilities,” SCA 9930, *Int. Symp. Soc. Core Analysts*, Golden, CO, USA, 1999.
 30. N. R. Nagarajan, M. M. Honarpour, and K. Sampath, “Comparison of Gas-Condensate Relative Permeability using live fluid vs. Model Fluids,” SCA 2004-009, *Int. Symp. Soc. Core Analysts*, Abu Dhabi, UAE, Oct. 5-9, 2004.
 31. S. Kalla, S. A. Leonardi, D. W. Berry, L. D. Poore, H. Sahoo, R. A. Kudva, and E. M. Braun, “Factors That Affect Gas-Condensate Relative Permeability,” *SPE Res. Eval. and Eng.*, vol. 18, no. 1, pp 5-10, Feb. 2015.
 32. A. Orangi, N. R. Nagarajan, M. M. Honarpour and J. Rosenzweig, “Unconventional Shale Oil and Gas-Condensate Reservoir Production, Impact of Rock, Fluid, and Hydraulic Fractures,” SPE 140536, *SPE Hydraul. Fracturing Technol. Conf. and Exhib.*, Woodlands, Texas, USA, Jan. 14-26, 2011.